Clinical and Translational Report

Cell Metabolism

Loss of Brain Aerobic Glycolysis in Normal Human Aging

Graphical Abstract

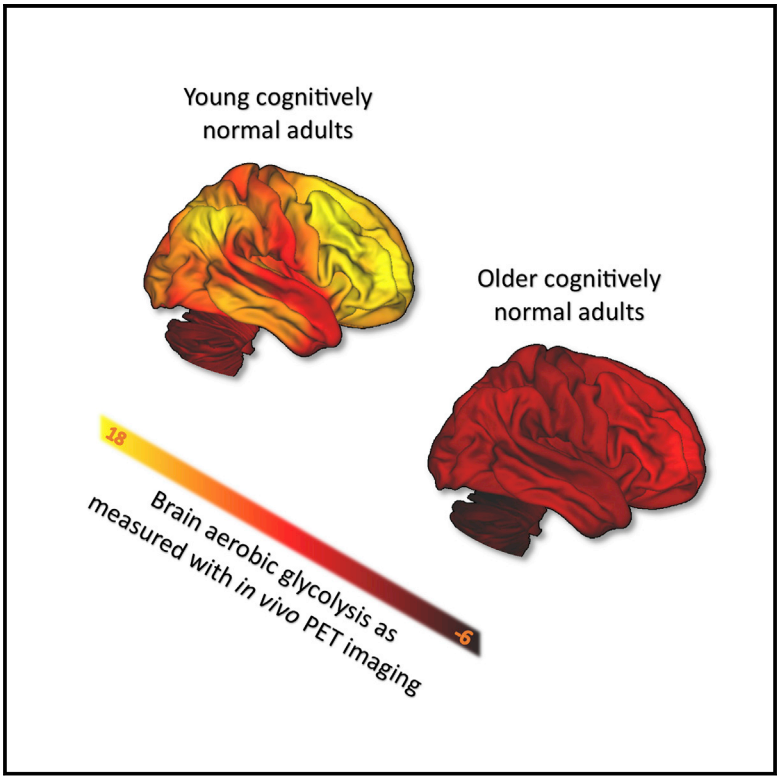

Highlights

- Whole-brain aerobic glycolysis (AG) falls with normal aging in humans
- The regional topography of brain AG changes significantly with normal aging
- Neotenous regions of the brain show the largest aging-related change in AG

Authors

Manu S. Goyal, Andrei G. Vlassenko, Tyler M. Blazey, ..., Tammie L.-S. Benzinger, John C. Morris, Marcus E. Raichle

Correspondence

goyalm@wustl.edu

In Brief

Prior work has shown that brain glucose metabolism falls with normal aging. Goyal et al. now find that this change in glucose metabolism is largely due to loss of aerobic glycolysis. Using PET imaging, they further demonstrate that the regional topography of brain aerobic glycolysis changes significantly with normal aging.

Goyal et al., 2017, Cell Metabolism *26*, 353–360
August 1, 2017
http://dx.doi.org/10.1016/j.cmet.2017.07.010

Cell Metabolism
Clinical and Translational Report

Loss of Brain Aerobic Glycolysis in Normal Human Aging

Manu S. Goyal,[1,2,3,4,5,*] Andrei G. Vlassenko,[1,3,4] Tyler M. Blazey,[1] Yi Su,[1,3] Lars E. Couture,[1] Tony J. Durbin,[1] Randall J. Bateman,[2,3] Tammie L.-S. Benzinger,[1,3] John C. Morris,[2,3] and Marcus E. Raichle[1,3]
[1]Mallinckrodt Institute of Radiology
[2]Department of Neurology
[3]Knight Alzheimer's Disease Research Center
Washington University School of Medicine, St. Louis, MO 63110, USA
[4]These authors contributed equally
[5]Lead Contact
*Correspondence: goyalm@wustl.edu
http://dx.doi.org/10.1016/j.cmet.2017.07.010

SUMMARY

The normal aging human brain experiences global decreases in metabolism, but whether this affects the topography of brain metabolism is unknown. Here we describe PET-based measurements of brain glucose uptake, oxygen utilization, and blood flow in cognitively normal adults from 20 to 82 years of age. Age-related decreases in brain glucose uptake exceed that of oxygen use, resulting in loss of brain aerobic glycolysis (AG). Whereas the topographies of total brain glucose uptake, oxygen utilization, and blood flow remain largely stable with age, brain AG topography changes significantly. Brain regions with high AG in young adults show the greatest change, as do regions with prolonged developmental transcriptional features (i.e., neoteny). The normal aging human brain thus undergoes characteristic metabolic changes, largely driven by global loss and topographic changes in brain AG.

INTRODUCTION

Normal aging is associated with changes in body appearance, physiology, and function, and likely arises from a combination of evolutionary trade-offs, environmental influences, and the natural degradation and failure of biological systems (Campisi, 2005; Kirkwood and Austad, 2000). The human brain also undergoes normal changes during aging, including loss in brain weight and volume (Dekaban, 1978; Fox and Schott, 2004; Scahill et al., 2003), cortical thickness (Salat et al., 2004; Sowell et al., 2003), and synaptic density (Huttenlocher, 1979; Masliah et al., 1993), and a global decrement in glucose metabolism, oxygen consumption, and cerebral blood flow (summarized in Goyal et al., 2014; Kety, 1956; Kuhl et al., 1982; Martin et al., 1991; Pantano et al., 1984). The reasons for these changes remain poorly understood. With regard to brain metabolism, it has been tacitly assumed that changes across the normal lifespan as measured by glucose metabolism or oxygen consumption, while rarely measured together, represent a decrease in the oxidative metabolism of glucose. Our data allow us to separate the non-oxidative and oxidative fractions of glucose use in the brain to determine whether this is true.

Human brain metabolism is unique in its high reliance on glucose utilization, which accounts for 20%–25% of the total body glucose consumption rate, though the brain comprises only 2% of typical human body mass (Mink et al., 1981; Raichle et al., 1970). These high metabolic rates are even higher during childhood development (summarized in Goyal et al., 2014). A characteristic feature of resting human brain glucose metabolism—particularly during development—is that it exceeds that required to account for its oxygen consumption rate by, on average, about 12%–15% in young adults (Boyle et al., 1994; Dastur, 1985; Raichle et al., 1970; Vaishnavi et al., 2010) and more in children (Goyal et al., 2014). This excess glucose utilization has been termed "aerobic glycolysis" (AG) in the human brain (Vaishnavi et al., 2010), following long-standing research on AG in cancer (Locasale and Cantley, 2011; Lunt and Vander Heiden, 2011). (To be precise, here we use the term "aerobic glycolysis" to refer to non-oxidative metabolism of glucose—including that which leads to lactate [i.e., the Warburg Effect] as well as other intermediary pathways that do not consume oxygen. As used historically, the term "aerobic glycolysis" refers to the fact that this occurs in the presence of oxygen, as opposed to "anaerobic glycolysis," which occurs in the absence of oxygen.) Several studies demonstrate that the release of lactate, a product of glycolysis, from the brain accounts for a portion of brain AG, but not its entirety (Glenn et al., 2015; Lubow et al., 2006; Madsen et al., 1995, 1999; Overgaard et al., 2012; Raichle et al., 1970), leading to the hypothesis that AG is likely also related to intermediary glucose metabolism, including that associated with biosynthesis and neuroprotection via the pentose phosphate pathway (Raichle, 2015; Vlassenko and Raichle, 2015). Recent studies suggest that brain AG might be particularly relevant for synaptic plasticity and learning (Goyal et al., 2014; Magistretti, 2016; Shannon et al., 2016).

The human brain is highly neotenous (Petanjek et al., 2011; Somel et al., 2009, 2014). Neoteny expresses the notion that during evolution, developmental processes are prolonged and potentiated beyond that seen relative to another species; in the brain, neoteny likely largely relates to prolonged periods of

synaptic plasticity, myelination, and other aspects of childhood brain development. We previously identified relative differences in transcriptional neoteny among human brain regions and found that regional AG—itself a developmental metabolic feature of the brain—correlates highly with transcriptional neoteny (Goyal et al., 2014). We therefore hypothesized that the waning of neotenous processes in the brain as a part of the normal aging process, such as decreasing synaptic plasticity and completion of myelination, would lead to measurable decreases in AG as the predominant feature of metabolic change in the aging human brain.

RESULTS AND DISCUSSION

To investigate this hypothesis, we first performed a meta-analysis of previously reported whole-brain measures of the cerebral metabolic rate of glucose use (CMRGlc), oxygen consumption ($CMRO_2$), and cerebral blood flow (CBF) across the adult lifespan to determine normative aging-related changes in whole-brain metabolism, including AG. We then applied these whole-brain measurements to independent PET regional measurements of glucose use, oxygen utilization, and cerebral blood flow in 205 cognitively normal adults spanning 20–82 years in age.

Whole-Brain AG Decreases with Age

Whole-brain measures of CMRGlc, $CMRO_2$, and CBF in cognitively normal individuals, derived largely from prior Kety-Schmidt-based methods (Kety and Schmidt, 1948) or quantitative PET imaging, were collected from the literature as previously described (Goyal et al., 2014) (Figure S1). These demonstrate an increase in all brain metabolism measures during childhood with a subsequent decrease during early adulthood. The decrease in CMRGlc continues during late adulthood, whereas whole-brain $CMRO_2$ and CBF remain relatively unchanged, as recently independently confirmed (Aanerud et al., 2017). AG represents the fraction of CMRGlc that is not metabolized by oxidative phosphorylation. Here we calculate AG by subtracting the fraction of CMRGlc accounted for by 6 molar equivalents of $CMRO_2$ from total CMRGlc. This is based on the 1:6 molar stoichiometric relationship between glucose and oxygen use in supplying oxidative phosphorylation. AG can be calculated at varying spatial levels: whole brain, region-wise, and at the level of individual voxels. Note that AG, as calculated in this manner, can be less than zero when substrates other than glucose, such as lactate, account for a portion of the measured $CMRO_2$.

When applying this calculation to loess fits of whole-brain CMRGlc and $CMRO_2$ across adulthood (Figure S1), we find that, on average, AG gradually decreases with age, approximating zero at the whole-brain level near the age of 60 (Figure 1). These findings are closely consistent with a prior quantitative Kety-Schmidt-based study in cognitively normal active young and older adults (Dastur, 1985).

Regional Changes in Brain AG: Study Participants and PET Data

Whole-brain group average assessment of aging-related changes in AG obscures regional and topographical changes that might also occur with age. In order to assess aging-related changes in regional differences in brain metabolism, we collected and curated PET imaging data from 205 cognitively normal adults participating in six different studies at our institution (Figure S2). All participants underwent PET imaging to determine brain CMRGlc, $CMRO_2$, CBF, and cerebral blood volume, and MRI for image registration and partial volume correction (see STAR Methods). Precise quantification of brain metabolism with PET typically requires invasive estimates of the arterial input function, which were not performed in this large cohort of 205 adults. As our intent here is to identify group average regional differences and inter-individual topographical changes, we instead combined literature-based whole estimates (Figure S1) with local-to-global ratios to determine quantitative regional values for each parameter of brain metabolism. Specifically, local-to-global ratios for CMRGlc, $CMRO_2$, and CBF were calculated for 79 gray and white matter brain regions and combined with the literature-based, age-specific whole-brain estimates to derive quantitative values for each metabolic parameter in each of the regions. These were then used to calculate regional AG as described above.

Significant outliers as determined by errors or marked deviations identified during preprocessing of the data were removed;

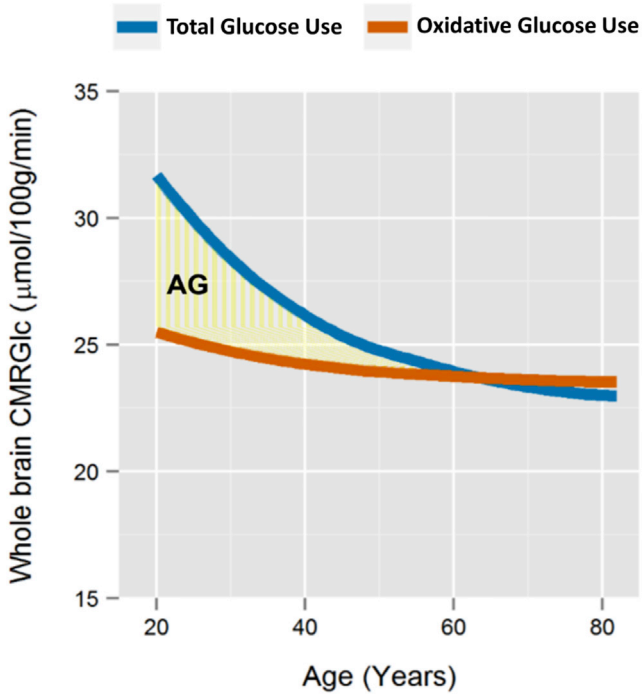

Figure 1. Meta-analysis of Human Whole-Brain Metabolism

We performed and fit loess curves to a meta-analysis of prior measurements of whole-brain CMRGlc ("total glucose use"; blue) and $CMRO_2$ converted to glucose use equivalents based on the stoichiometric oxygen-to-glucose ratio of 6 ("oxidative glucose use"; orange) (see Figure S1 for details). This shows that CMRGlc decreases significantly with age, but $CMRO_2$ does not change or only minimally so, resulting in gradual decrease in apparent whole-brain AG (yellow shaded region). Apparent whole-brain AG approximates zero near the age of 60. Notably, similar changes in whole-brain AG between young (mean 21 years old) and older (mean 71 years old) individuals were noted by Darab Dastur in 1985 based on multiple Kety-Schmidt measurements (Dastur, 1985), when restricting the older cohort to "physically and mentally active" healthy participants.

no outliers were removed after commencing group statistical analysis. Of the remaining 205 participants, 29 underwent repeat PET imaging between 1 and 2 years later, including 19 that were amyloid imaging negative. All participants reported normal cognitive status and were verbally screened at recruitment for significant neurological or mental health illness. Nearly all participants above the age of 35 (n = 157, excluding 3 participants aged 44, 58, and 60) underwent brain amyloid imaging and were found to have either a CDR of 0 and/or normal results on Short Blessed and AD8 testing. Participants with positive amyloid imaging were excluded from further analyses to highlight normative changes in brain metabolism; thus, the primary normative cohort described below includes 184 PET sessions in 165 participants.

The Topography of Brain Metabolism Changes Characteristically with Age

We first applied quantile normalization across the 184 individual PET sessions in the primary normative cohort with respect to each metabolic parameter (CMRGlc, $CMRO_2$, CBF, and AG) independently. For an arbitrary set of data points within any particular data sample, quantile normalization assigns the same reference quantitative values to each data point according to its rank within the sample, thereby preserving the rank order of the data points yet normalizing its statistical distribution without presuming a statistical distribution a priori (Bolstad et al., 2003). This method is often used in other large data domains to correct, for example, batch effects in gene expression data. In this case, quantile normalization forces the region-wise data from each PET session to match one another in their quantitative histogram. Whereas this alters the absolute quantitative values for independent data points, individual differences in the topography of brain metabolism are preserved. Note that this method also effectively erases differences in the statistical distribution (e.g., mean and SD) arising from differences between PET scanners or study type.

We applied principal component analysis and multidimensional scaling to the normalized data. The data are sufficiently complex that a minimum of 53 principal components are required to explain just 75% of the variance. However, the samples largely map according to participant age (Figure S3). Participant age correlates with the first principal coordinate (PC1), demonstrating that the topography, i.e., regional configuration, of brain metabolism changes significantly with age (PC1, $r = 0.56$, $p < 2 \times 10^{-16}$; PC2, $r = -0.11$, $p = 0.14$). The sex and/or gender of the participant also modestly relates to the first principal coordinate (female versus male PC1, $t = -2.75$, $p < 0.007$; PC2, $t = -0.93$, $p = 0.35$).

AG Accounts for Much of the Aging-Related Topographic Changes in Brain Metabolism

How do the individual forms of metabolism drive the topographic, i.e., region-wise, changes identified above? The rank order of brain regions according to a parameter of metabolism reflects the topography of that parameter of brain metabolism. To further investigate aging-related changes in brain metabolism topography, we determined how Spearman rank correlations between individuals and an average baseline map from young adults (ages 20–23) vary with age. While the rank correlations

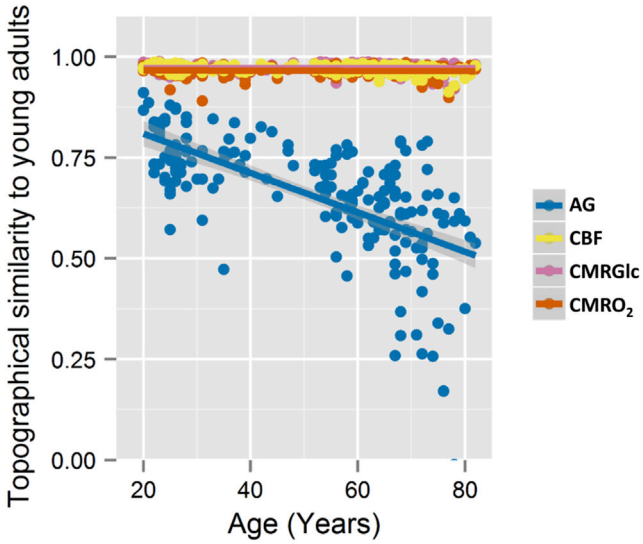

Figure 2. Brain AG Topography Changes with Normal Human Aging

The normalized data for each metabolic parameter and each individual were Spearman rank correlated with an average dataset comprising participants aged 20–23 years. For CBF (yellow), CMRGlc (pink), and $CMRO_2$ (orange), the Spearman rank correlation remained high throughout the lifespan (CMRGlc minimum Spearman's rho = 0.92, $CMRO_2$ min rho = 0.89, CBF min rho = 0.91), suggesting that the topography for these aspects of brain metabolism remain relatively stable throughout the adult lifespan. The Spearman rank correlations for AG (blue) for each participant instead show significant decreases with age (Pearson's $r = -0.64$, $p < 2 \times 10^{-16}$), remaining only modestly similar to the young adults among the oldest participants. High inter-individual variability is evident for AG, particularly among the older participants. These changes in AG topography are in part due to whole-brain changes in AG and in part due to topographical changes between CMRGlc and $CMRO_2$ (see Figure S4 for details).

remain high for CMRGlc, $CMRO_2$, and CBF throughout the adult lifespan and across individuals (CMRGlc minimum Spearman's rho = 0.92, $CMRO_2$ min rho = 0.89, CBF min rho = 0.91), AG topography changes significantly with age, becoming more and more dissimilar to young adult brain metabolism (age versus AG topography rank correlations, Pearson's $r = -0.64$, $p < 2 \times 10^{-16}$) (Figure 2). Multivariate analysis confirms that aging-related differences in brain metabolism topography are dominated by AG topography, though the topography of other parameters changes slightly also with age (multivariate general linear model, AG, $p < 2 \times 10^{-16}$; CBF, $p = 0.0002$; CMRGlc, $p < 0.00001$; $CMRO_2$, $p = 0.07$). These results indicate that whereas the topography of CMRGlc, $CMRO_2$, and CBF remains relativity stable during normal aging, brain AG topography varies considerably with age. This topography is not completely lost, however; the topography of brain metabolism remains somewhat similar even in the most aged participants as compared to our youngest participants.

These topographic changes mirror quantitative changes in whole-brain AG. Indeed, much of the changes in brain AG topography may be due to quantitative differences in whole-brain AG. Alternatively or in addition, brain AG changes might be due to aging-associated changes in the topographic relationship between CMRGlc and $CMRO_2$, which theoretically can occur independently of differences in whole-brain CMRGlc and $CMRO_2$. To

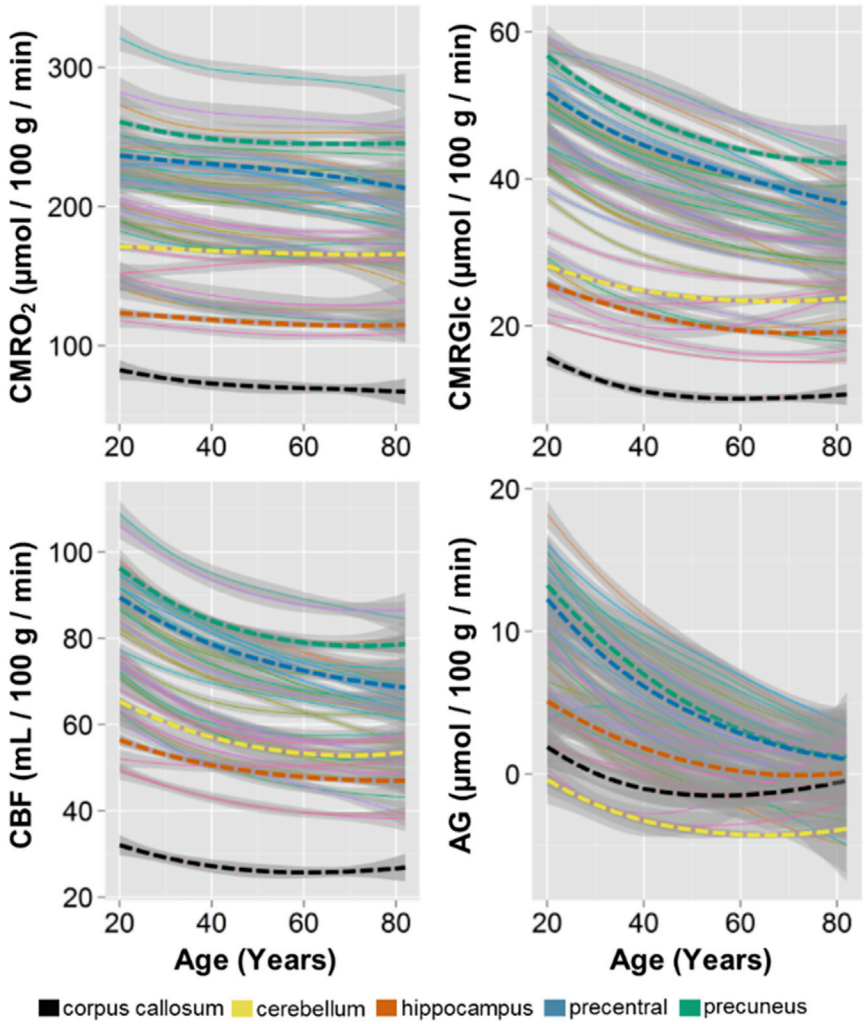

Figure 3. Summary of Regional Quantitative Metabolic Change in the Human Brain with Aging

Literature-based whole-brain estimates for $CMRO_2$, CMRGlc, CBF, and AG were combined with local-to-global ratios to determine a quantitative value in every individual in the normative cohort, for each metabolic parameter in 42 gray matter regions and the corpus callosum as a representative white matter region. These were then fit with loess curves to demonstrate the trajectory for each metabolic parameter in each of these regions. The thin lines represent each of the regions with superimposed thick dotted lines representing representative regions, as shown in the bottom legend. The shaded gray regions show the SE about the loess curves, though it should be noted that using literature-based whole-brain estimates will necessarily obscure quantitative inter-individual variability. It is evident that, with rare exception, all regions decrease in all aspects of metabolism. However, the loss of $CMRO_2$ is slight as compared to the more dramatic decrease in AG, which regionally varies in rate of change with aging. This whole-brain normalized regionally quantitative data are provided as a normative dataset in Data S1.

explore these possibilities further, we calculated the Glycolytic Index (GI) across brain regions for each PET session. GI is calculated by determining the residuals after spatially regressing $CMRO_2$ from CMRGlc (Vaishnavi et al., 2010); in effect, this identifies the topographic linear dissimilarity between CMRGlc and $CMRO_2$ and is thus independent of whole-brain quantitative measures of metabolism. Here we find that brain GI topography also decreases significantly with age (Pearson's $r = -0.20$, $p < 0.006$), though not to the same degree as AG (Figure S4). This result suggests that changes in brain AG topography are likely due to both quantitative differences in whole-brain AG and changes in the topographic relationship between CMRGlc and $CMRO_2$.

Neotenous Brain Regions Show the Most Change in AG

Till now, the analysis on the normative cohort has been limited to quantile normalized data, which represent the topography of brain metabolism. Here we now address the non-normalized data, which were derived by combining local-to-global PET imaging measurements of CMRGlc, $CMRO_2$, and CBF with whole-brain literature-based estimates, and calculating AG from the regional quantitative values of CMRGlc and $CMRO_2$. We then applied loess fits to each independent region across the group. This method results in a diverse set of trajectories for AG, CMRGlc, $CMRO_2$, and CBF across all of the cortical and subcortical gray matter regions, the cerebellum, and the corpus callosum (Figure 3). Comparison of these quantitative regional AG values among sex- and/or gender-matched young (21–35 year olds) and older adults (60–76 year olds) reveals several differences (Figure 4). In addition to an overall decrease in quantitative AG, there is a "flattening" of AG across regions such that the topography of AG is readily apparent in young adults, but less so in older adults. We thus hypothesized that the degree of aging-related change in a particular region would be related to its AG in young adulthood.

Across 42 cortical and subcortical gray matter regions and the cerebellum, aging-related change in AG highly correlates with the degree of AG in the same regions at the start of adulthood (regional AG in young adults aged 20–23 years versus slope of change in AG, Pearson's $r = -0.87$, $p < 3 \times 10^{-14}$) (Figure 5A). Further, our prior work (Goyal et al., 2014) demonstrated that regions with high AG during young adulthood correlate with transcriptional neoteny, i.e., the relative persistence of gene expression that is characteristic of childhood development. The measurement of transcriptional neoteny in each region is restricted to the 16 regions assessed in the BrainSpan data (Kang et al., 2011) and used in our study (Goyal et al., 2014), including the cerebellum, which is used as the reference region. Among these regions, the aging-related regional decrease in AG correlates also with transcriptional neoteny (regional neoteny index versus slope of change in AG, Pearson's $r = -0.79$, $p < 0.0005$) (Figure 5B).

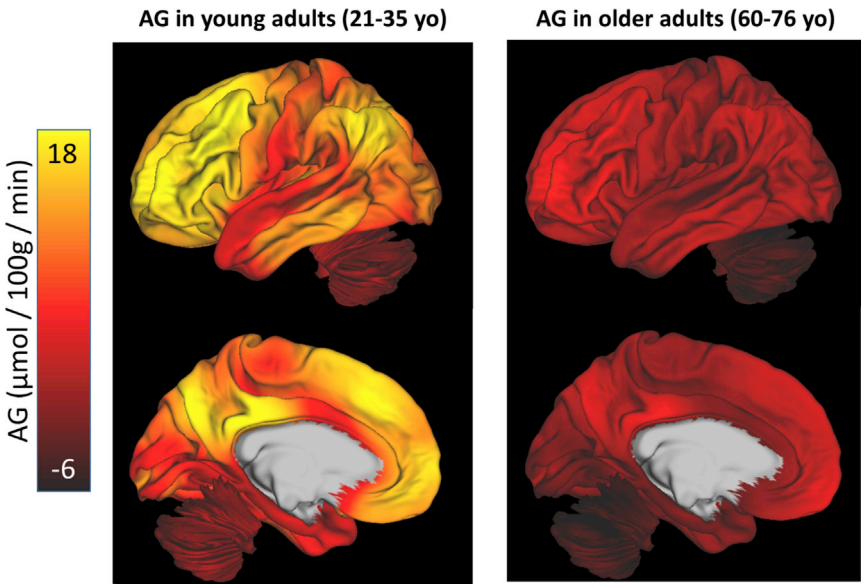

Figure 4. The Topography of AG Flattens with Aging

Quantitative values for AG were determined by combining literature-based whole-brain values for CMRGlc and $CMRO_2$ with local-to-global values within each individual (see STAR Methods). This demonstrates that in a young cohort of adults (21–35 years old), AG varies considerably throughout the brain as has been described previously (Vaishnavi et al., 2010). In an older cohort (60–76 years old) matched for sex and/or gender, the overall topography of AG is flattened and depressed. Slight regional variation of AG persists in a manner similar to that seen in young adults, accounting for the modestly positive Spearman rank correlations for older adults (Figure 2). As our measurement of AG does not include other carbohydrate use for oxidative phosphorylation—such as lactate—some values of AG extend below zero, in particular in the cerebellum in the older cohort.

Collectively, these results suggest that aging-related changes in AG predominantly occur in the most neotenous regions of the human brain.

AG Loss as a Biomarker of Human Brain Aging

Our findings thus demonstrate that brain AG and its initial topography in young adults gradually wane with normal aging, particularly in the most neotenous regions of the brain. These changes occur in the absence of amyloid pathology or neurologically evident brain pathology, suggesting that they represent a "baseline mode" of normal brain metabolism aging. The aging-related loss of AG identified here might both represent underlying physiologic changes and harbor ill consequences to the aging brain.

Why does whole-brain AG fall with age? The molecular and cellular drivers of AG in the normal human brain are not currently known. Lactate release from the brain, such as that arising from AG in the astrocyte, likely accounts for a significant portion of measured AG in the human brain (Glenn et al., 2015; Lubow et al., 2006; Madsen et al., 1995, 1999; Overgaard et al., 2012; Raichle et al., 1970). The reason for net lactate release from the human brain is unclear, but rapid ATP production and volume transmission of metabolic states have been raised as putative explanations (Bergersen and Gjedde, 2012), and lactate might also have a role in potentiating the hemodynamic response locally by increasing the NADH/NAD+ ratio (Mintun et al., 2004).

However, current estimates of whole-brain net lactate release in young adults are not sufficient to account for the degree of whole-brain AG identified here, suggesting that intermediary metabolism of glucose may also play a role in human brain metabolism (Goyal et al., 2014; Lunt and Vander Heiden, 2011). Intermediary metabolism of glucose could support neotenous processes by providing substrates directly for myelin, glycolipids, and protein synthesis (Goyal et al., 2014) and/or fueling microglia in their increasingly recognized role in synaptic elimination and homeostasis (Magistretti, 2016; Shannon et al., 2016). Whereas the apportionment of brain AG to different metabolic pathways is likely complex and requires further investigation, the decrease in AG with age may in part correspond to decreases in synaptic and myelin development with age. Loss of dendritic spine turnover with age has been shown in rodents with two-photon imaging studies (Holtmaat et al., 2005; Yang et al., 2009; Zuo et al., 2005). Similarly, synaptic and spine density falls in the human brain with age, which may be associated with decreased expression of genes related to synaptic and spine development and increased expression of genes related to myelination and spine growth inhibition (Goyal and Raichle, 2013). It is currently unknown whether aging-related regional changes in cortical myelination correspond to the regional changes in brain AG identified here, but new methods and data such as that arising from the Lifespan Extension to the Human Connectome Project can directly test this hypothesis (Glasser et al., 2014).

The aging-related loss of AG may also portend a loss of neuroprotection via the pentose phosphate pathway against oxidative stress, increasing the risk for oxidative damage. Many aging-related conditions of the brain are associated with oxidative stress, including neurodegenerative diseases such as Parkinson disease and Alzheimer's disease. AG-related neuroprotection might normally counter the potential costs of heightened synaptic plasticity in the brain, but in the aging brain the loss of such neuroprotection could lead to heightened damage from reactive oxygen species. If true, we would predict that the neotenous regions of the human brain, i.e., regions with initially high brain AG, would be particularly vulnerable to such forms of damage, perhaps helping to explain the link between late developing regions and their vulnerability to neurodegeneration (Douaud et al., 2014).

One limitation of our study is that it does not include measurements of brain carbohydrate consumption beyond glucose. The human brain is known to be able to use lactate and ketones for oxidative metabolism, and studies suggest that in some scenarios the human brain to some extent prefers lactate over glucose (Dienel, 2012; Smith et al., 2003). One possible explanation for some of the aging-related loss of brain AG is that the aging brain may gradually switch its carbohydrate preference to lactate

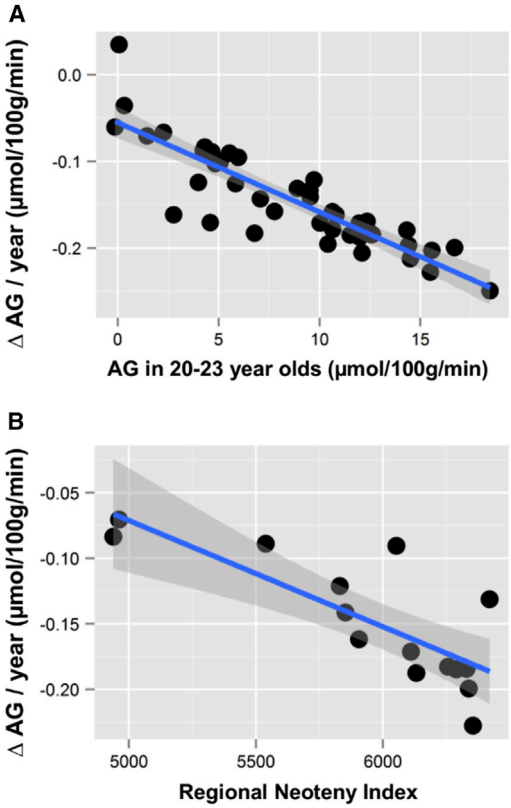

Figure 5. Regional Rate of Decreased AG Correlates with Regional Metabolic and Transcriptional Neoteny

(A) AG was calculated for each region using the combined literature-based whole-brain and local-to-global values (see STAR Methods). Change in AG per year was then calculated for each region and compared to the AG in that region in young adults aged 20–23 years. Regions with the highest AG in young adults showed the most rapid loss of AG per year (Pearson's $r = -0.87$, $p < 3 \times 10^{-14}$), including such regions as the medial frontal cortex and the precuneus.

(B) The BrainSpan lifespan human brain transcriptional data were used to calculate a regional neoteny index, which is a measure of the persistence of developmentally related gene expression (Goyal et al., 2014), for each of the 15 regions assessed by the BrainSpan dataset as compared to the cerebellum. In addition to the cerebellum, the 15 regions include dorsolateral prefrontal cortex; ventrolateral, medial, and orbital frontal cortex; primary motor, somatosensory, auditory, and visual cortex; posterior inferior parietal cortex; posterior superior and inferior temporal cortex; hippocampus and amygdala; striatum; and thalamus (Kang et al., 2011). The loss of AG per year for these 15 regions inversely correlates with their regional neoteny index (Pearson's $r = -0.79$, 95% CI -0.47 to -0.93, $p < 0.0005$). These results suggest that the largest aging-related change in AG occurs in the most metabolic and transcriptionally neotenous regions of the human brain, accounting for the flattening of AG seen in Figure 4.

for oxidative metabolism. Studies of aging-related differences in brain lactate uptake would be helpful to investigate this possibility further. Changes in cerebral blood flow and vascular disease might further contribute to aging-related changes in AG and warrant further investigation. We also caution that our regional analysis of human brain AG relies on FDG-PET imaging. Though FDG has long been held as an appropriate marker of regional glucose metabolism in the human brain, exploring regional brain AG with other methods such as ^{11}C-glucose PET or ^{13}C-glucose MR spectroscopy might be helpful.

Importantly, our results demonstrate that studies of brain aging that are restricted to measuring total glucose use or cerebral blood flow are missing important aging-related changes in brain metabolism, including that of AG. The normative data here are provided as a supplement for future research investigations and in comparison to extant and ongoing brain aging-related data. As for cancer (Liberti and Locasale, 2016), the roles and apportionment of brain AG remain unclear and require further investigation. Comparing these data to genetic and molecular findings in humans and mechanistic findings in non-human animals may help further reveal why brain AG changes with age and reveal its consequences.

STAR★METHODS

Detailed methods are provided in the online version of this paper and include the following:

- KEY RESOURCES TABLE
- CONTACT FOR REAGENT AND RESOURCE SHARING
- EXPERIMENTAL MODEL AND SUBJECT DETAILS
  - Human Participants
- METHOD DETAILS
  - MRI
  - Amyloid PET Imaging
  - CMRGlc, $CMRO_2$ and CBF PET Imaging
- QUANTIFICATION AND STATISTICAL ANALYSIS
  - Image Analysis
  - FreeSurfer Analysis
  - Partial Volume Correction
  - Quantitative Calculations of Regional Parameters
  - AG Measurement
  - Statistics
- DATA AND SOFTWARE AVAILABILITY
  - Raw, Age-Normalized, Brain Metabolism Data in Cognitively Normal Adults
  - R Script and Data
  - Imaging Data
- ADDITIONAL RESOURCES

SUPPLEMENTAL INFORMATION

Supplemental Information includes four figures and one data file and can be found with this article online at http://dx.doi.org/10.1016/j.cmet.2017.07.010.

AUTHOR CONTRIBUTIONS

Conceptualization and Methodology, M.S.G., A.G.V., and M.E.R.; Formal Analysis, M.S.G., A.G.V., T.M.B., Y.S., and L.E.C.; Investigation, all authors; Data Curation, M.S.G., A.G.V., L.E.C., and T.J.D.; Writing – Original Draft, M.S.G., A.G.V., and M.E.R.; Writing – Review & Editing, all authors; Supervision and Funding Acquisition, A.G.V., T.L.-S.B., J.C.M., and M.E.R.

CONFLICTS OF INTEREST

The authors declare no conflicts of interest.

ACKNOWLEDGMENTS

We are continually grateful for our participants' time and effort in this and other studies. We are also thankful for useful discussions on this work with Anish Mitra and Dr. Avi Snyder. The data presented here were the result of several

independently funded efforts, including grants from the Barnes-Jewish Hospital Foundation, Charles F. and Joanne Knight, the James S. McDonnell Foundation, and the McDonnell Center for Systems Neuroscience (22-3922-26239N); the Radiological Society of North America; and the NIH (NS06833, NS057901, NS048056, MH077967, P50AG005681, P01AG003991, P01AG26276, UF1AG032438, UL1TR000448, P30NS098577, and R01EB009352).

Received: January 23, 2017
Revised: May 25, 2017
Accepted: July 17, 2017
Published: August 1, 2017

REFERENCES

Aanerud, J., Borghammer, P., Rodell, A., Jónsdottir, K.Y., and Gjedde, A. (2017). Sex differences of human cortical blood flow and energy metabolism. J. Cereb. Blood Flow Metab. *37*, 2433–2440.

Bergersen, L.H., and Gjedde, A. (2012). Is lactate a volume transmitter of metabolic states of the brain? Front. Neuroenergetics *4*, 5.

Bolstad, B.M., Irizarry, R.A., Astrand, M., and Speed, T.P. (2003). A comparison of normalization methods for high density oligonucleotide array data based on variance and bias. Bioinformatics *19*, 185–193.

Boyle, P.J., Scott, J.C., Krentz, A.J., Nagy, R.J., Comstock, E., and Hoffman, C. (1994). Diminished brain glucose metabolism is a significant determinant for falling rates of systemic glucose utilization during sleep in normal humans. J. Clin. Invest. *93*, 529–535.

Brix, G., Zaers, J., Adam, L.E., Bellemann, M.E., Ostertag, H., Trojan, H., Haberkorn, U., Doll, J., Oberdorfer, F., and Lorenz, W.J.; National Electrical Manufacturers Association (1997). Performance evaluation of a whole-body PET scanner using the NEMA protocol. J. Nucl. Med. *38*, 1614–1623.

Campisi, J. (2005). Senescent cells, tumor suppression, and organismal aging: good citizens, bad neighbors. Cell *120*, 513–522.

Dastur, D.K. (1985). Cerebral blood flow and metabolism in normal human aging, pathological aging, and senile dementia. J. Cereb. Blood Flow Metab. *5*, 1–9.

Dekaban, A.S. (1978). Changes in brain weights during the span of human life: relation of brain weights to body heights and body weights. Ann. Neurol. *4*, 345–356.

Desikan, R.S., Ségonne, F., Fischl, B., Quinn, B.T., Dickerson, B.C., Blacker, D., Buckner, R.L., Dale, A.M., Maguire, R.P., Hyman, B.T., et al. (2006). An automated labeling system for subdividing the human cerebral cortex on MRI scans into gyral based regions of interest. Neuroimage *31*, 968–980.

Dienel, G.A. (2012). Brain lactate metabolism: the discoveries and the controversies. J. Cereb. Blood Flow Metab. *32*, 1107–1138.

Douaud, G., Groves, A.R., Tamnes, C.K., Westlye, L.T., Duff, E.P., Engvig, A., Walhovd, K.B., James, A., Gass, A., Monsch, A.U., et al. (2014). A common brain network links development, aging, and vulnerability to disease. Proc. Natl. Acad. Sci. USA *111*, 17648–17653.

Fischl, B., Salat, D.H., Busa, E., Albert, M., Dieterich, M., Haselgrove, C., van der Kouwe, A., Killiany, R., Kennedy, D., Klaveness, S., et al. (2002). Whole brain segmentation: automated labeling of neuroanatomical structures in the human brain. Neuron *33*, 341–355.

Fischl, B., van der Kouwe, A., Destrieux, C., Halgren, E., Ségonne, F., Salat, D.H., Busa, E., Seidman, L.J., Goldstein, J., Kennedy, D., et al. (2004). Automatically parcellating the human cerebral cortex. Cereb. Cortex *14*, 11–22.

Fox, N.C., and Schott, J.M. (2004). Imaging cerebral atrophy: normal ageing to Alzheimer's disease. Lancet *363*, 392–394.

Fox, P.T., Raichle, M.E., Mintun, M.A., and Dence, C. (1988). Nonoxidative glucose consumption during focal physiologic neural activity. Science *241*, 462–464.

Frouin, V., Comtat, C., Reilhac, A., and Grégoire, M.C. (2002). Correction of partial-volume effect for PET striatal imaging: fast implementation and study of robustness. J. Nucl. Med. *43*, 1715–1726.

Glasser, M.F., Goyal, M.S., Preuss, T.M., Raichle, M.E., and Van Essen, D.C. (2014). Trends and properties of human cerebral cortex: correlations with cortical myelin content. Neuroimage *93*, 165–175.

Glenn, T.C., Martin, N.A., Horning, M.A., McArthur, D.L., Hovda, D.A., Vespa, P., and Brooks, G.A. (2015). Lactate: brain fuel in human traumatic brain injury: a comparison with normal healthy control subjects. J. Neurotrauma *32*, 820–832.

Goyal, M.S., and Raichle, M.E. (2013). Gene expression-based modeling of human cortical synaptic density. Proc. Natl. Acad. Sci. USA *110*, 6571–6576.

Goyal, M.S., Hawrylycz, M., Miller, J.A., Snyder, A.Z., and Raichle, M.E. (2014). Aerobic glycolysis in the human brain is associated with development and neotenous gene expression. Cell Metab. *19*, 49–57.

Graham, M.M., Muzi, M., Spence, A.M., O'Sullivan, F., Lewellen, T.K., Link, J.M., and Krohn, K.A. (2002). The FDG lumped constant in normal human brain. J. Nucl. Med. *43*, 1157–1166.

Holtmaat, A.J., Trachtenberg, J.T., Wilbrecht, L., Shepherd, G.M., Zhang, X., Knott, G.W., and Svoboda, K. (2005). Transient and persistent dendritic spines in the neocortex in vivo. Neuron *45*, 279–291.

Huttenlocher, P.R. (1979). Synaptic density in human frontal cortex—developmental changes and effects of aging. Brain Res. *163*, 195–205.

Kang, H.J., Kawasawa, Y.I., Cheng, F., Zhu, Y., Xu, X., Li, M., Sousa, A.M., Pletikos, M., Meyer, K.A., Sedmak, G., et al. (2011). Spatio-temporal transcriptome of the human brain. Nature *478*, 483–489.

Kety, S.S. (1956). Human cerebral blood flow and oxygen consumption as related to aging. J. Chronic Dis. *3*, 478–486.

Kety, S.S., and Schmidt, C.F. (1948). The nitrous oxide method for the quantitative determination of cerebral blood flow in man: theory, procedure and normal values. J. Clin. Invest. *27*, 476–483.

Kirkwood, T.B., and Austad, S.N. (2000). Why do we age? Nature *408*, 233–238.

Kuhl, D.E., Metter, E.J., Riege, W.H., and Phelps, M.E. (1982). Effects of human aging on patterns of local cerebral glucose utilization determined by the [18F] fluorodeoxyglucose method. J. Cereb. Blood Flow Metab. *2*, 163–171.

Lancaster, J.L., Glass, T.G., Lankipalli, B.R., Downs, H., Mayberg, H., and Fox, P. (1995). A modality-independent approach to spatial normalization of tomographic images of the human brain. Hum. Brain Mapp. *3*, 209–223.

Liberti, M.V., and Locasale, J.W. (2016). The Warburg effect: how does it benefit cancer cells? Trends Biochem. Sci. *41*, 211–218.

Locasale, J.W., and Cantley, L.C. (2011). Metabolic flux and the regulation of mammalian cell growth. Cell Metab. *14*, 443–451.

Lubow, J.M., Piñón, I.G., Avogaro, A., Cobelli, C., Treeson, D.M., Mandeville, K.A., Toffolo, G., and Boyle, P.J. (2006). Brain oxygen utilization is unchanged by hypoglycemia in normal humans: lactate, alanine, and leucine uptake are not sufficient to offset energy deficit. Am. J. Physiol. Endocrinol. Metab. *290*, E149–E153.

Lunt, S.Y., and Vander Heiden, M.G. (2011). Aerobic glycolysis: meeting the metabolic requirements of cell proliferation. Annu. Rev. Cell Dev. Biol. *27*, 441–464.

Madsen, P.L., Hasselbalch, S.G., Hagemann, L.P., Olsen, K.S., Bülow, J., Holm, S., Wildschiødtz, G., Paulson, O.B., and Lassen, N.A. (1995). Persistent resetting of the cerebral oxygen/glucose uptake ratio by brain activation: evidence obtained with the Kety-Schmidt technique. J. Cereb. Blood Flow Metab. *15*, 485–491.

Madsen, P.L., Cruz, N.F., Sokoloff, L., and Dienel, G.A. (1999). Cerebral oxygen/glucose ratio is low during sensory stimulation and rises above normal during recovery: excess glucose consumption during stimulation is not accounted for by lactate efflux from or accumulation in brain tissue. J. Cereb. Blood Flow Metab. *19*, 393–400.

Magistretti, P.J. (2016). Imaging brain aerobic glycolysis as a marker of synaptic plasticity. Proc. Natl. Acad. Sci. USA *113*, 7015–7016.

Martin, W.R., Powers, W.J., and Raichle, M.E. (1987). Cerebral blood volume measured with inhaled C15O and positron emission tomography. J. Cereb. Blood Flow Metab. *7*, 421–426.

Martin, A.J., Friston, K.J., Colebatch, J.G., and Frackowiak, R.S. (1991). Decreases in regional cerebral blood flow with normal aging. J. Cereb. Blood Flow Metab. *11*, 684–689.

Masliah, E., Mallory, M., Hansen, L., DeTeresa, R., and Terry, R.D. (1993). Quantitative synaptic alterations in the human neocortex during normal aging. Neurology *43*, 192–197.

Mink, J.W., Blumenschine, R.J., and Adams, D.B. (1981). Ratio of central nervous system to body metabolism in vertebrates: its constancy and functional basis. Am. J. Physiol. *241*, R203–R212.

Mintun, M.A., Raichle, M.E., Martin, W.R., and Herscovitch, P. (1984). Brain oxygen utilization measured with O-15 radiotracers and positron emission tomography. J. Nucl. Med. *25*, 177–187.

Mintun, M.A., Vlassenko, A.G., Rundle, M.M., and Raichle, M.E. (2004). Increased lactate/pyruvate ratio augments blood flow in physiologically activated human brain. Proc. Natl. Acad. Sci. USA *101*, 659–664.

Mintun, M.A., Larossa, G.N., Sheline, Y.I., Dence, C.S., Lee, S.Y., Mach, R.H., Klunk, W.E., Mathis, C.A., DeKosky, S.T., and Morris, J.C. (2006). [11C]PIB in a nondemented population: potential antecedent marker of Alzheimer disease. Neurology *67*, 446–452.

Morris, J.C. (1993). The Clinical Dementia Rating (CDR): current version and scoring rules. Neurology *43*, 2412–2414.

Overgaard, M., Rasmussen, P., Bohm, A.M., Seifert, T., Brassard, P., Zaar, M., Homann, P., Evans, K.A., Nielsen, H.B., and Secher, N.H. (2012). Hypoxia and exercise provoke both lactate release and lactate oxidation by the human brain. FASEB J. *26*, 3012–3020.

Pantano, P., Baron, J.C., Lebrun-Grandié, P., Duquesnoy, N., Bousser, M.G., and Comar, D. (1984). Regional cerebral blood flow and oxygen consumption in human aging. Stroke *15*, 635–641.

Petanjek, Z., Judaš, M., Šimic, G., Rasin, M.R., Uylings, H.B., Rakic, P., and Kostovic, I. (2011). Extraordinary neoteny of synaptic spines in the human prefrontal cortex. Proc. Natl. Acad. Sci. USA *108*, 13281–13286.

Raichle, M.E. (2015). The restless brain: how intrinsic activity organizes brain function. Philos. Trans. R. Soc. Lond. B Biol. Sci. *370*, http://dx.doi.org/10.1098/rstb.2014.0172.

Raichle, M.E., Posner, J.B., and Plum, F. (1970). Cerebral blood flow during and after hyperventilation. Arch. Neurol. *23*, 394–403.

Raichle, M.E., Martin, W.R., Herscovitch, P., Mintun, M.A., and Markham, J. (1983). Brain blood flow measured with intravenous H2(15)O. II. Implementation and validation. J. Nucl. Med. *24*, 790–798.

Salat, D.H., Buckner, R.L., Snyder, A.Z., Greve, D.N., Desikan, R.S., Busa, E., Morris, J.C., Dale, A.M., and Fischl, B. (2004). Thinning of the cerebral cortex in aging. Cereb. Cortex *14*, 721–730.

Scahill, R.I., Frost, C., Jenkins, R., Whitwell, J.L., Rossor, M.N., and Fox, N.C. (2003). A longitudinal study of brain volume changes in normal aging using serial registered magnetic resonance imaging. Arch. Neurol. *60*, 989–994.

Shannon, B.J., Vaishnavi, S.N., Vlassenko, A.G., Shimony, J.S., Rutlin, J., and Raichle, M.E. (2016). Brain aerobic glycolysis and motor adaptation learning. Proc. Natl. Acad. Sci. USA *113*, E3782–E3791.

Smith, D., Pernet, A., Hallett, W.A., Bingham, E., Marsden, P.K., and Amiel, S.A. (2003). Lactate: a preferred fuel for human brain metabolism in vivo. J. Cereb. Blood Flow Metab. *23*, 658–664.

Somel, M., Franz, H., Yan, Z., Lorenc, A., Guo, S., Giger, T., Kelso, J., Nickel, B., Dannemann, M., Bahn, S., et al. (2009). Transcriptional neoteny in the human brain. Proc. Natl. Acad. Sci. USA *106*, 5743–5748.

Somel, M., Rohlfs, R., and Liu, X. (2014). Transcriptomic insights into human brain evolution: acceleration, neutrality, heterochrony. Curr. Opin. Genet. Dev. *29*, 110–119.

Sowell, E.R., Peterson, B.S., Thompson, P.M., Welcome, S.E., Henkenius, A.L., and Toga, A.W. (2003). Mapping cortical change across the human life span. Nat. Neurosci. *6*, 309–315.

Su, Y., D'Angelo, G.M., Vlassenko, A.G., Zhou, G., Snyder, A.Z., Marcus, D.S., Blazey, T.M., Christensen, J.J., Vora, S., Morris, J.C., et al. (2013). Quantitative analysis of PiB-PET with FreeSurfer ROIs. PLoS One *8*, e73377.

Su, Y., Blazey, T.M., Snyder, A.Z., Raichle, M.E., Marcus, D.S., Ances, B.M., Bateman, R.J., Cairns, N.J., Aldea, P., Cash, L., et al.; Dominantly Inherited Alzheimer Network (2015). Partial volume correction in quantitative amyloid imaging. Neuroimage *107*, 55–64.

Vaishnavi, S.N., Vlassenko, A.G., Rundle, M.M., Snyder, A.Z., Mintun, M.A., and Raichle, M.E. (2010). Regional aerobic glycolysis in the human brain. Proc. Natl. Acad. Sci. USA *107*, 17757–17762.

Vlassenko, A.G., and Raichle, M.E. (2015). Brain aerobic glycolysis functions and Alzheimer's disease. Clin. Transl. Imaging *3*, 27–37.

Vlassenko, A.G., Vaishnavi, S.N., Couture, L., Sacco, D., Shannon, B.J., Mach, R.H., Morris, J.C., Raichle, M.E., and Mintun, M.A. (2010). Spatial correlation between brain aerobic glycolysis and amyloid-β (Aβ) deposition. Proc. Natl. Acad. Sci. USA *107*, 17763–17767.

Yang, G., Pan, F., and Gan, W.B. (2009). Stably maintained dendritic spines are associated with lifelong memories. Nature *462*, 920–924.

Zuo, Y., Lin, A., Chang, P., and Gan, W.B. (2005). Development of long-term dendritic spine stability in diverse regions of cerebral cortex. Neuron *46*, 181–189.

STAR★METHODS

KEY RESOURCES TABLE

REAGENT or RESOURCE	SOURCE	IDENTIFIER
Deposited Data		
Regional, age-normalized, partial volume corrected brain metabolism data in 165 individuals across 184 PET sessions	This paper	http://dx.doi.org/10.17632/hh2c2gtzpy.1
Regional, age-normalized, partial volume corrected brain metabolism data in 205 individuals across 234 PET sessions	This paper	http://dx.doi.org/10.17632/hwgvf99r7h.1
Raw imaging data for all 234 PET sessions	This paper	Available upon request only
Software and Algorithms		
FreeSurfer	Martinos Center for Biomedical Imaging, Massachusetts General Hospital/Harvard-MIT Health Sciences & Technology	https://surfer.nmr.mgh.harvard.edu
R	The R Project for Statistical Computing	https://www.r-project.org
R Script and Data	R script and data for key statistical results (raw imaging data not included)	http://dx.doi.org/10.17632/hwgvf99r7h.1

CONTACT FOR REAGENT AND RESOURCE SHARING

Further information and requests for data and resources (except for data that is restricted for access due to sensitive medical information) should be directed to and will be fulfilled by the Lead Contact, Manu S. Goyal (goyalm@wustl.edu).

EXPERIMENTAL MODEL AND SUBJECT DETAILS

Human Participants

A total of 205 individuals (59% women, self-reported sex / gender) aged 20-82 years were recruited from the Washington University community and the Knight Alzheimer Disease Research Center (ADRC). All participants had no neurological, psychiatric, or systemic medical illness that might compromise study participation. Individuals were excluded if they had contraindications to MRI, history of mental illness, possible pregnancy, or medication use that could interfere with brain function. All studies in participants coming from the Knight ADRC projects (n = 157 studies) included cognitive assessments, neurological evaluations, and clinical assessments and were cognitively normal based on the Clinical Dementia Rating (CDR) (Morris, 1993). Participants may have participated in other procedures related to the study that they were involved with, beyond those described here.

All assessments and imaging procedures were approved by Human Research Protection Office and Radioactive Drug Research Committee at Washington University in St. Louis. Written consent was provided from each participant.

METHOD DETAILS

MRI

MRI scans were obtained in all individuals to guide anatomical localization. High-resolution structural images were acquired at 1.5T (Vision, Siemens, Erlangen, Germany) or 3T (Siemens TIM Trio) scanner using a 3D sagittal T1-weighted magnetization-prepared 180° radio-frequency pulses and rapid gradient-echo (MPRAGE) sequence (typical parameters: TE = 3.93ms, TR = 1900ms, TI = 1100ms, flip angle = 20°, 256 × 256 acquisition matrix, 160 slices, 1 × 1 x 1-1.3 mm voxels).

Amyloid PET Imaging

All participants older than 35 years, excluding 3 (aged 44, 58, and 60, final n = 157) underwent a 60 min dynamic Pittsburgh compound B (PIB) PET scan following injection of ~10 mCi PIB. The PIB PET imaging procedure has been described in detail (Mintun et al., 2006; Su et al., 2013), and was conducted with a Siemens model 962 ECAT EXACT HR+ PET scanner (Siemens/CTI, Knoxville, KY) or on a Siemens Biograph 40 PET/CT scanner (Siemens/CTI, Knoxville, KY). Standard uptake value ratios (SUVR) with the cerebellar cortex as reference were calculated from regions of interest with PIB-positivity defined as the mean cortical SUVR (from predefined prefrontal, parietal, and temporal regions of interest) > 1.42, a value commensurate with a mean cortical binding potential of 0.18 as defined previously for a similar cohort (Mintun et al., 2006).

CMRGlc, $CMRO_2$ and CBF PET Imaging

In all but 20 individuals ^{18}F-FDG and ^{15}O PET scans were performed on a Siemens model 962 ECAT EXACT HR+ PET scanner (Siemens/CTI, Knoxville, KY) (Brix et al., 1997) and in 20 individuals, ^{18}F-FDG scans were performed on a Siemens Biograph 40 PET/CT scanner on the same or next day or (in one case) 7 weeks later to measure CMRGlc following the same protocols we have described previously (Vaishnavi et al., 2010; Vlassenko et al., 2010).

All individuals underwent one FDG scan and either one or two ^{15}O PET scans. FDG scans were performed after slow intravenous injection of 5 mCi of FDG to measure CMRGlc (Fox et al., 1988). Venous samples for plasma glucose determination were obtained just before and at the midpoint of the scan to verify that glucose levels were within normal range throughout the study. Dynamic acquisition of PET emission data continued for 60 min with twenty five 5 s frames, nine 20 s frames, ten 1 min frames, and nine 5 min frames. The last 20 min were summed to create the CMRGlc image (Fox et al., 1988; Vaishnavi et al., 2010; Vlassenko et al., 2010).

In individuals with two replicates of ^{15}O scans, CBV, CBF, and $CMRO_2$, values were averaged for data analysis. Each ^{15}O PET scan included sets of three ^{15}O scans (CO, H_2O, and O_2) to measure CBV, CBF, and $CMRO_2$ (Martin et al., 1987; Mintun et al., 1984; Raichle et al., 1983). The $CMRO_2$ parametric image was derived from the ^{15}O PET scans and corrected for CBV, using a previously described method (Vaishnavi et al., 2010; Vlassenko et al., 2010).

CBV was measured with a 5 min emission scan beginning 2 min after brief inhalation of 75 mCi of [^{15}O]CO in room air as described previously (Martin et al., 1987). Dynamic scans of 3 min with thirty five 2 s frames, six 5 s frames, and eight 10 s frames were acquired after injection of 50 mCi [^{15}O]H_2O in saline or inhalation of 60 mCi of [^{15}O]O_2 in room air, respectively for CBF and $CMRO_2$ measurements. By creating a whole-brain time-activity curve, the onset of activity in the brain could be judged exactly, allowing for a consistent selection of the optimal 40 s frame, over which activity was summed. These registrations and their corresponding transformations were performed with in-house software. Individual head movement during scanning was restricted by a thermoplastic mask. All PET images were acquired in the eyes-closed waking state. No specific instructions were given regarding cognitive activity during scanning other than to remain awake.

QUANTIFICATION AND STATISTICAL ANALYSIS

Image Analysis

The PET scans were registered to each other and then to the individual's MRI scan, which was in turn registered to an atlas representative target image, corresponding to Talairach space as defined by Lancaster et al. (Lancaster et al., 1995). The PET images were blurred and resampled into atlas space. These registrations and their corresponding transformations were performed with in-house software. Using an atlas derived brain mask, each individual's CMRGlc, CBV, CBF, and $CMRO_2$ images were scaled to have whole brain means of 1, and then same mode images, if they existed were averaged.

FreeSurfer Analysis

FreeSurfer software (Desikan et al., 2006; Fischl et al., 2002, 2004) was used to segment the brain into well-defined cortical and subcortical, gray and white matter regions of interest (ROIs) based on individual MPRAGE MRI scans. These ROIs were used for regional estimation of PET parameters.

Partial Volume Correction

MR based partial volume correction of PET data was performed using regional spread function approach (Frouin et al., 2002), based on FreeSurfer defined ROIs (Su et al., 2015).

Quantitative Calculations of Regional Parameters

The local-to-global images obtained as described above for CMRGlc, $CMRO_2$, and CBF were summarized to the FreeSurfer defined gray and white matter brain regions. These were then multiplied by age-specific literature-based whole brain estimates derived from loess fits for each of the metabolic parameters. Theoretically, obtaining individual Kety-Schmidt whole brain metabolism measurements alongside their PET studies might have resulted in more accurate results. However, such an invasive study would be extraordinarily expensive in over 100 participants and of questionable ethical permissibility; for example, a recent attempt to use the Kety-Schmidt method in normal adults was rejected by our Institutional Review Board on the basis that such measurements are available in the literature. Alternatively, quantitative estimates using PET have been often obtained by placing an arterial line to measure an arterial input function, which is then applied to a model to determine quantitative regional parameters; however, in addition to being invasive and likely not feasible in more than a few dozen participants, this method depends upon model assumptions that vary across studies and centers, including a lumped constant which itself is reliant on literature-based Kety-Schmidt based measurements (Graham et al., 2002). Thus, while our method here may not be accurate at an individual level, it is likely more accurate for group-wise results as it takes advantage of data from several prior studies, and certainly more feasible in a sample size sufficiently large to identify robust aging related changes.

AG Measurement

We evaluated three measures of AG: 1) oxygen/glucose index (OGI) defined by voxel-wise division of relative $CMRO_2$ by the relative CMRGlc; 2) AG defined by subtracting the oxidative fraction of CMRGlc, calculated by dividing molar $CMRO_2$ by six from total molar CMRGlc ($AG = CMRGlc - CMRO_2 \div 6$); and 3) GI defined by the residuals after spatially regressing $CMRO_2$ from CMRGlc (Vaishnavi et al., 2010). These three measures are highly correlated in our data. However OGI may be very noisy in areas of low CMRGlc as it is in the denominator, and GI does not yield interpretable quantitative values. Therefore, AG is used as the primary measure of aerobic glycolysis and has the further intuitive appeal of being larger when there is increased aerobic glycolysis, in contrast to the more historically used OGI.

Statistics

Significance was defined as $p < 0.05$. Aside from image analysis, all statistics reported in this study were calculated in R version 3.1.1.

DATA AND SOFTWARE AVAILABILITY

Raw, Age-Normalized, Brain Metabolism Data in Cognitively Normal Adults

A CSV file (AgeNormalizedBrainMetabolism.csv) is provided as Data S1, which contains regional, age-normalized, partial volume corrected values for CMRGlc, $CMRO_2$, CBF, and AG for each of the 184 PET sessions in the 165 amyloid-negative individuals, as a normative dataset of brain metabolism in adults.

R Script and Data

The R script and associated R data (which includes the data contained in the CSV file above) have been deposited to Mendeley Data and are available at http://dx.doi.org/10.17632/hwgvf99r7h.1 to reproduce key findings in this manuscript. The R script was used for data normalization, summary statistics and to produce several of the graphs in this manuscript.

Imaging Data

The raw imaging data and/or imaging preprocessing scripts used in this study can be obtained upon request to the Lead Contact.

ADDITIONAL RESOURCES

A portion of the data came from the Dominantly Inherited Alzheimer Network (DIAN) observational trial (https://clinicaltrials.gov/; Identifier: NCT00869817) and from the ongoing Adult Children Study; further information on these studies can be obtained at http://www.dian-info.org/ and http://alzheimer.wustl.edu/Volunteer/ACS.html.